

Adaptive Negativity Estimation via Collective Measurements

Martin Zeman,^{1,2,*} Vojtěch Trávníček,^{2,†} Antonín Černocho,^{2,‡} Jan Soubusta,^{1,§} and Karel Lemr^{1,¶}

¹Palacký University in Olomouc, Faculty of Science,
Joint Laboratory of Optics of Palacký University and Institute of Physics AS CR,
17. listopadu 12, 771 46 Olomouc, Czech Republic

²Institute of Physics of the Academy of Sciences of the Czech Republic,
Joint Laboratory of Optics of Palacký University and Institute of Physics AS CR,
17. listopadu 50a, 772 07 Olomouc, Czech Republic

(Dated: March 27, 2026)

This paper explores an efficient method for entanglement quantification in two-qubit and qubit-qutrit quantum systems based upon the framework of collective measurements in conjunction with machine learning. We introduce an adaptive measurement procedure in which measurement settings are dynamically adjusted based on prior measurement outcomes aiming to optimize the inference precision given a limited number of these measurement settings. The procedure makes use of the Long Short-Term Memory networks to recurrently process collective measurements on two copies of the investigated states. Obtained results demonstrate the tangible benefits of the adaptive measurements in comparison to previously described non-adaptive strategies.

INTRODUCTION

Quantum entanglement is a fundamental consequence of the superposition principle applied to multipartite quantum states [1]. It has been studied for nearly a century [2–4], but despite all efforts, developing a method for its experimentally feasible quantification in general quantum systems remains a challenging and complex problem [5, 6]. The ultimate aim is to create an approach that minimizes the number of necessary measurements while maximizing the detection accuracy, thus rendering the process more efficient and practical for deployment in quantum technologies.

There is a broad portfolio of entanglement quantifiers among which the quantum state negativity is prominently used for its beneficial characteristics such as being an entanglement monotone and measure [7]. Negativity extends the Peres-Horodecki criterion, which is a necessary and, in some cases, sufficient condition for the presence of entanglement in quantum systems [8–10]. Having access only to single-copy measurements on the tested state, negativity needs to be calculated from the density matrix [11] reconstructed in the process of a complete quantum state tomography [12, 13]. This process is hampered by the unfavorable scaling of measurement configurations that increase quadratically with the Hilbert space dimension.

An alternative approach towards entanglement estimation is based on collective measurements which are simultaneous (and generally nonlocal) measurements implemented on multiple copies of the tested state [14–19]. It has been shown that by performing a m -copy collective measurement, one gets access to the m th order moment of the density matrix which is needed to calculate negativity of a m -dimensional state [20–22]. The drawback of this procedure is the experimental unattainability of such a complex measurement [23]. However, one can limit one-

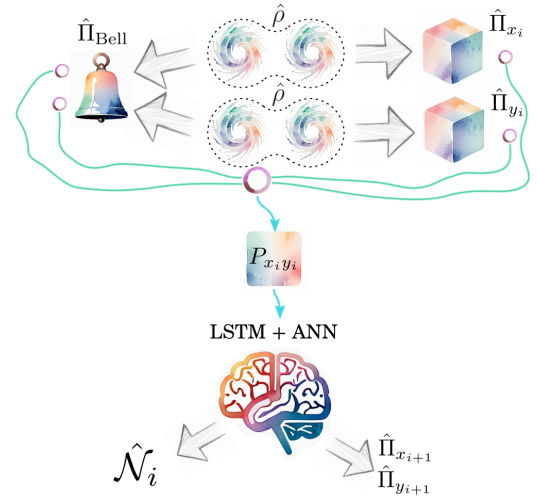


FIG. 1. The conceptual diagram of a two-copy collective measurement and subsequent negativity prediction by artificial neural network (ANN) model with Long Short-Term Memory (LSTM) cells. Two instances of the system under investigation, denoted as $\hat{\rho}$, are measured simultaneously. During the measurement, one subsystem from each instance undergoes a local projection using operators $\hat{\Pi}_{x_i}$ and $\hat{\Pi}_{y_i}$, while the other two subsystems are non-locally projected using the $\hat{\Pi}_{\text{Bell}}$ operator. The results of these measurements, denoted as $P_{x_i y_i}$, are sequentially used as inputs for the ANN, which then after each measurement estimates the negativity $\hat{\mathcal{N}}_i$ of $\hat{\rho}$ and recommends the most suitable local measurements for the next iteration $\hat{\Pi}_{x_{i+1}}$ and $\hat{\Pi}_{y_{i+1}}$.

self to only two-copy collective measurements and still obtain a reasonably precise negativity estimation while maintaining the number of measurement configurations reduced with respect to the full quantum state tomography [24, 25]. The concept of such collective measurement is depicted in Fig. 1. The approximate estimate for negativity obtained from the two-copy collective measure-

ments can then be obtained by harnessing the universal approximation power of artificial neural networks [26].

Moreover, this approach is particularly relevant because the experimental configuration for two-copy collective measurements closely mirrors the entanglement swapping protocol [27]. This protocol constitutes a critical mechanism for quantum repeaters and relays [28, 29], which are essential components of quantum communication networks [30]. Two-copy collective measurements have been used, for example, for quantum relay diagnostics [31], quantum metrology [32] or machine learning [33] tasks.

In our previous research, the results of collective measurements were processed by fully connected neural networks to estimate the negativity in two-qubit and qubit-qutrit quantum states [24, 25, 34–36]. However, the parameters of these measurements were determined in advance and were therefore state independent. In this work, we extend this approach by introducing adaptive measurements, in which the settings of subsequent measurements are dynamically adjusted based on the outcomes of previous measurements.

Adaptive quantum measurements are known to be an efficient tool for extracting useful information from a quantum state [37]. Their efficiency is measured in terms of obtained precision while requiring less resources (fewer measurements, smaller samples or shorter computation time) with respect to non-adaptive approaches. Adaptive methods started being developed for the purposes of the quantum state tomography and estimation [38–40]. Originally, the algorithms were based on the Bayes’ rule [41, 42], which is recently being replaced by neural networks [43, 44]. Apart from the quantum state tomography, adaptive measurements outperform their non-adaptive counterparts in quantum phase estimation [45–47], entanglement detection [48, 49] or quantum communications [50].

As we document in later sections, the combination of adaptive and collective measurements leads to a tangible improvement in the precision of negativity estimation for a given number of measurement configurations. The recurrent nature of this task requires a shift from fully connected neural networks to recurrent neural networks (RNN). In this work, we employ the Long Short-Term Memory (LSTM) network, a specialized type of RNN designed to identify and retain patterns in sequential data [51]. LSTM networks are particularly effective in overcoming the vanishing gradient problem [52], which makes them well suited for adaptive quantum measurement tasks. It should be stressed out that once a model is trained, its daily operation is significantly faster than the algorithms based on the Bayes’ rule [43].

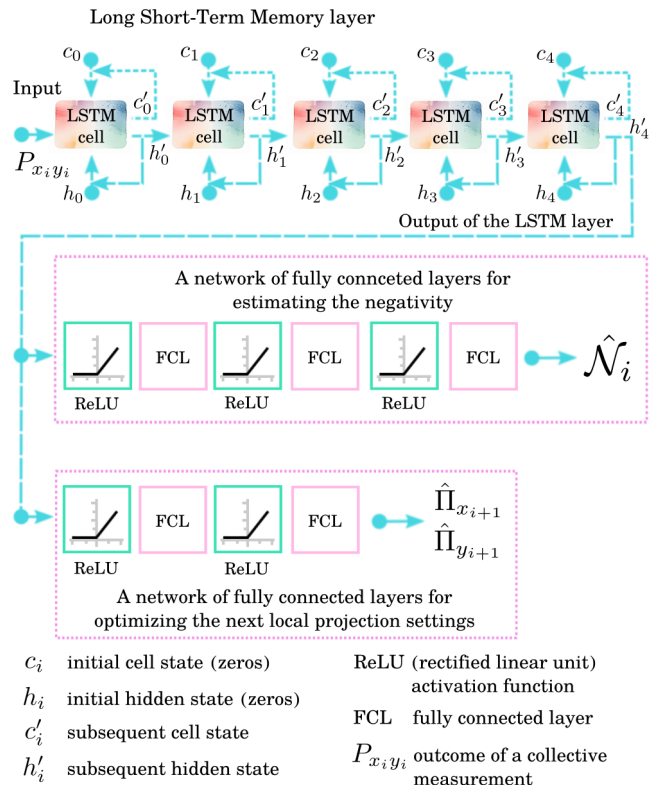


FIG. 2. Topology of the artificial neural network for the negativity $\hat{\mathcal{N}}_i$ estimation and for the prediction of the next set of local measurements $\hat{\Pi}_{x_{i+1}}$, $\hat{\Pi}_{y_{i+1}}$. The LSTM cell states and hidden states are 128 32-bit integers long while the size of the hidden fully connected layers is 256.

METHODS

Our goal is to infer the value of negativity from an adaptively iterated series of collective measurements. As indicated in the introduction, we focus on collective measurements applied to two copies of the investigated state. More specifically, to two copies of (i) a two-qubit and (ii) a qubit-qutrit state. This choice is motivated by a prominent role of the negativity which is for these states a necessary and sufficient entanglement witness as well as an entanglement measure [7].

The investigated state is described by its density matrix $\hat{\rho}$. Thus, the two copies of the state can be described simply as a direct product

$$\hat{\Omega} = \hat{S}^T \hat{\rho} \hat{S} \otimes \hat{\rho}, \quad (1)$$

where \hat{S} stands for the operator swapping subsystems in the density matrix of the first copy ($\hat{\rho}_{AB} \xrightarrow{\hat{S}} \hat{\rho}_{BA}$). The role of the swapping operator \hat{S} will become evident in subsequent derivations.

The collective measurement itself consists of a local and nonlocal part described by two local projectors $\hat{\Pi}_x$

and $\hat{\Pi}_y$ acting on the same subsystems across the two copies (see conceptual diagram in Fig. 1). The remaining two subsystems are simultaneously projected onto a common entangled (non-local) state denoted by the projector $\hat{\Pi}_{\text{Bell}}$. We chose the projector on the fully anti-symmetric two-qubit subspace

$$\hat{\Pi}_{\text{Bell}} = |\Psi^-\rangle\langle\Psi^-|, \quad |\Psi^-\rangle = \frac{1}{\sqrt{2}}(|01\rangle - |10\rangle) \quad (2)$$

to be the fixed non-local projector. In case of the qubit-qutrit states, the non-local projection is performed to the qubit subsystems. The outcome of the collective measurement is an overall projection probability expressed as

$$P_{xy} = \text{Tr}[\hat{\Omega}(\hat{\Pi}_x \otimes \hat{\Pi}_{\text{Bell}} \otimes \hat{\Pi}_y)]. \quad (3)$$

This equation illustrates how the swap operator \hat{S} ensures correct ordering of the subsystems. Typically, one chooses a single nonlocal projector $\hat{\Pi}_{\text{Bell}}$ (or POVM operator in a more general case) and repeats the measurement for a sequence of different local projectors $\{\hat{\Pi}_{x_i} \otimes \hat{\Pi}_{y_i}\}$. Thus, one obtains a sequence of probabilities $\{P_{x_i y_i}\}$. Negativity or other quantity of interest is then inferred from this sequence. Note that the probabilities P_{xy} are experimentally accessible since Eq. (3) can be directly implemented. In practice, the measurement is repeated with many instances of $\hat{\Omega}$ to estimate the probabilities with sufficient precision.

The sequence of local operators is fixed in the case of a non-adaptive procedure. In this paper, we present an adaptive procedure, in which the local projectors imposed on the state in the $(i+1)$ th iteration step are proposed based on the results of the i previous measurements. We make use of a neural network model consisting of both recurrent LSTM cells and fully connected layers to estimate negativity from the total of i collective measurements ($P_{x_1 y_1}, P_{x_2 y_2}, \dots, P_{x_i y_i}$) and also to predict the optimal local projectors for the $(i+1)$ th iteration ($\hat{\Pi}_{x_{i+1}}$ and $\hat{\Pi}_{y_{i+1}}$). The entire neural network model is schematically visualized in Fig. 2.

We label $\hat{\mathcal{N}}_i(\hat{\rho})$ the *negativity estimate* of state $\hat{\rho}$ after the total of i collective measurements have been performed. For purposes of training and testing of our models, we analytically calculate the *true negativity*

$$\mathcal{N}(\hat{\rho}) = \left| \sum_{\lambda_j < 0} \lambda_j \right|, \quad (4)$$

where λ_j denote the eigenvalues of a partially transposed density matrix $\hat{\rho}^\Gamma$.

Training and testing of models

The training and testing of the models started by generating random two-qubit or qubit-qutrit states using the

method described in [53]. Each model is trained on a set of 2^{18} random states that were split into mini-batches \mathcal{B} of size B . The input features of the model consist of the collective measurement probabilities P_{xy} obtained by applying Eq. (3) to each density matrix $\hat{\Omega}$. One input feature per density matrix is calculated in each iteration of the model (labeled $i = 1, \dots, n$). In the first iteration, a fixed set of local projectors $\Pi_{x_1} = \Pi_{y_1} = |0\rangle\langle 0|$ is applied. For the next iterations $i = 2, \dots, n$, the model proposes new pairs of local projectors (Π_{x_i} and Π_{y_i}) independently for every density matrix. In addition to the newly proposed local projectors, in every iteration, the model outputs the negativity estimate $\hat{\mathcal{N}}_i(\hat{\rho})$ corresponding to each investigated state.

Once all iterations $i = 2, \dots, n$ are complete for one mini-batch of density matrices, back-propagation and parameter updates are performed using the Adam optimizer with a learning rate of 0.001. We implemented two different loss functions, serving as figures of merit during training. Based on the selected loss function, we distinguish the *greedy* approach

$$\mathcal{L}_{\text{greedy}}^{(2)}(n) = \frac{1}{nB} \sum_{\hat{\rho} \in \mathcal{B}} \sum_{i=1}^n \left(\hat{\mathcal{N}}_i(\hat{\rho}) - \mathcal{N}(\hat{\rho}) \right)^2 \quad (5)$$

and the *last* approach

$$\mathcal{L}_{\text{last}}^{(2)}(n) = \frac{1}{B} \sum_{\hat{\rho} \in \mathcal{B}} \left(\hat{\mathcal{N}}_n(\hat{\rho}) - \mathcal{N}(\hat{\rho}) \right)^2. \quad (6)$$

Both loss functions are ordinary $\mathcal{L}^{(2)}$ distances between the predicted and true negativity values. The difference is that, in the case of the *greedy* algorithm, the model is optimized based on its intermediate negativity predictions made in each iteration. Conversely, models trained using the *last* approach are only optimized based on the final negativity prediction. The *greedy* models' parameters generally converge faster, and the models are easier to train. *Last* models are more difficult to train and fail more frequently during training. However, if successful, they offer better final negativity estimates. This procedure is repeated for every mini-batch, thus completing the training epoch.

To prevent overfitting, a separate validation set of 2^{16} random density matrices is generated and used to assess the model performance after each epoch. If no improvement on the validation set is detected for 10 consecutive epochs, the size of the mini-batches increases by a factor of two starting from $B = 32$ until it reaches its maximum value $B = 512$ [54]. Training is then terminated and the best-performing model is saved for testing. The models are tested on a third and independent set of 2^{16} random density matrices. The results are presented in subsequent sections.

The entire procedure described was coded in the Python programming language using the PyTorch library

[55] to implement the models and their training. All programming code, final trained models and testing results can be accessed on Figshare [56].

RESULTS

As indicated in the Methods section, two different approaches based on two different loss functions designated *greedy* (5) and *last* (6) were tested. On top of that, we trained the neural networks using an optimal fixed (*non-adaptive*) set of bases. Non-adaptive training and operation of the models was simply achieved by overriding the usage of model-proposed basis in every iteration by a fixed basis from a list. These bases and their ordering were chosen according to previous research [34, 36]. Comparing the performance of adaptive models with models trained with a non-adaptive set of bases allows quantifying the improvement gained by the models' adaptability.

We have selected two quantifiers to assess the performance of the models. Straightforwardly, one can make use of the $\mathcal{L}^{(1)}$ distance between the true and estimated negativity averaged over the entire testing set \mathcal{T} (of size T)

$$\mathcal{L}^{(1)}(n) = \frac{1}{T} \sum_{\hat{\rho} \in \mathcal{T}} |\hat{\mathcal{N}}_n(\hat{\rho}) - \mathcal{N}(\hat{\rho})|. \quad (7)$$

Unlike the $\mathcal{L}^{(2)}$ distance used for training, the $\mathcal{L}^{(1)}$ distance has a simpler physical interpretation as the deviation of the predicted negativity from its true value. The second quantifier used is the coefficient of determination R^2 describing the variance of the estimated values of negativity with respect to the true values

$$R^2(n) = 1 - \frac{\sum_{\hat{\rho} \in \mathcal{T}} (\hat{\mathcal{N}}_n(\hat{\rho}) - \mathcal{N}(\hat{\rho}))^2}{\sum_{\hat{\rho} \in \mathcal{T}} (\hat{\mathcal{N}}_n(\hat{\rho}) - \langle \hat{\mathcal{N}}_n \rangle)^2}, \quad (8)$$

where $\langle \hat{\mathcal{N}}_n \rangle$ is the predicted value of negativity averaged over the training set.

For every set of parameters such as the number of iterations or the loss function type, a series of at least five models were trained to obtain the performance statistics. A model is deemed successfully trained if, for a given number of iterations n , it performs better in terms of the $\mathcal{L}^{(1)}$ distance than any other model trained on less iterations. Otherwise the model is discarded. We present both the mean performance over the entire set of successful models as well as the performance of the best model.

Two-qubit states

First, we present the results concerning two-qubit states. The qubit-qutrit systems are discussed afterward.

TABLE I. Numerical results for two-qubit systems using an adaptive *greedy* measurement strategy as a function of the number of n iterations. The figures of merit $\mathcal{L}^{(1)}$ and R^2 are defined in the main text.

n	$\mathcal{L}^{(1)}$ mean	$\mathcal{L}^{(1)}$ best	R^2 mean	R^2 best
2	0.0900(03)	0.0895	0.5952(67)	0.6003
3	0.0405(02)	0.0402	0.9070(13)	0.9095
4	0.0315(11)	0.0302	0.9419(67)	0.9470
5	0.0225(04)	0.0217	0.9690(11)	0.9700
6	0.0179(03)	0.0173	0.9806(09)	0.9818
7	0.0146(16)	0.0125	0.9869(25)	0.9900
8	0.0118(02)	0.0114	0.9912(04)	0.9915
9	0.0105(06)	0.0097	0.9929(07)	0.9940
10	0.0092(04)	0.0083	0.9942(05)	0.9953

TABLE II. Numerical results for two-qubit systems using an adaptive *last* measurement strategy as a function of the number of n iterations. The figures of merit $\mathcal{L}^{(1)}$ and R^2 are defined in the main text.

n	$\mathcal{L}^{(1)}$ mean	$\mathcal{L}^{(1)}$ best	R^2 mean	R^2 best
2	0.0902(04)	0.0896	0.5969(47)	0.5896
3	0.0401(02)	0.0399	0.9077(16)	0.9084
4	0.0248(18)	0.0238	0.9628(41)	0.9651
5	0.0180(29)	0.0145	0.9801(59)	0.9871
6	0.0111(05)	0.0105	0.9920(07)	0.9929
7	0.0096(03)	0.0092	0.9937(05)	0.9942
8	0.0083(01)	0.0082	0.9951(02)	0.9952
9	0.0076(02)	0.0074	0.9955(02)	0.9958
10	0.0070(01)	0.0068	0.9960(01)	0.9961

Tables I and II summarize the performance statistics of the models trained using the *greedy* and *last* approaches, respectively. The rows correspond to the number of iterations n ranging from 2 to 10; the case $n = 1$ is excluded due to its incompatibility with the adaptive measurement framework. The upper limit of $n = 10$ measurement configurations corresponds to the maximum number of independent collective measurements available for a two-qubit system [36], which follows directly from the symmetry of the density matrix $\hat{\Omega}$.

For comparison, the performance of equivalent non-adaptive models using an optimal sequence of fixed bases is summarized in Tables III and IV. The performance of the best adaptive and non-adaptive models, as described by $\mathcal{L}^{(1)}(n)$, is visualized in Fig. 3 as a function of the number of iterations n . Additionally, we plot two-dimensional histograms of the estimated and true negativity values in Fig. 4 for several selected parameters. These histograms were obtained by processing samples of 4096 random states. The separable states (zero valued negativity) are accumulated in the first bin.

Our results indicate that, as expected, the adaptive models outperform their non-adaptive counterparts across the entire range of iteration steps until $n = 10$. The convergence at $n = 10$ is expected since this corre-

TABLE III. Numerical results for two-qubit systems using a non-adaptive optimal basis set and the *greedy* estimation approach. Here, n denotes the number of iterations. The figures of merit $\mathcal{L}^{(1)}$ and R^2 are defined in the main text.

n	$\mathcal{L}^{(1)}$ mean	$\mathcal{L}^{(1)}$ best	R^2 mean	R^2 best
2	0.1049(08)	0.1037	0.5363(58)	0.5406
3	0.0588(05)	0.0582	0.8124(21)	0.8112
4	0.0484(02)	0.0481	0.8702(14)	0.8720
5	0.0382(03)	0.0380	0.9152(03)	0.9155
6	0.0250(02)	0.0247	0.9616(06)	0.9623
7	0.0211(00)	0.0210	0.9721(07)	0.9728
8	0.0175(04)	0.0169	0.9800(05)	0.9808
9	0.0119(03)	0.0116	0.9909(06)	0.9916
10	0.0084(03)	0.0081	0.9951(03)	0.9953

TABLE IV. Numerical results for two-qubit systems using a non-adaptive optimal basis set and the *last* estimation approach. Here, n denotes the number of iterations. The figures of merit $\mathcal{L}^{(1)}$ and R^2 are defined in the main text.

n	$\mathcal{L}^{(1)}$ mean	$\mathcal{L}^{(1)}$ best	R^2 mean	R^2 best
2	0.1059(05)	0.1053	0.5331(65)	0.5257
3	0.0588(04)	0.0581	0.8144(16)	0.8161
4	0.0483(02)	0.0481	0.8712(23)	0.8709
5	0.0382(01)	0.0381	0.9155(10)	0.9153
6	0.0249(02)	0.0246	0.9619(05)	0.9625
7	0.0208(02)	0.0206	0.9725(03)	0.9729
8	0.0166(03)	0.0163	0.9814(04)	0.9821
9	0.0105(02)	0.0102	0.9923(04)	0.9928
10	0.0068(01)	0.0067	0.9960(02)	0.9961

sponds to the maximum number of unbiased measurement configurations. Moreover, the adaptive models trained using the *last* approach outperform the *greedy* models as they minimize the error solely at the last iteration step. In contrast, the *greedy* models are optimized to provide reasonable estimates at every iteration. Conversely, we did not observe any significant difference in performance between the *greedy* and *last* non-adaptive models.

The presented results highlight the tangible benefits of using the adaptive measurement strategy. For example, at $n = 5$ the average deviation between the true negativity and its estimate made by the best available adaptive model is only 0.0145, which is more than $2.5\times$ smaller than that of the best available non-adaptive model (0.0380). It should also be noted that negativity cannot be analytically calculated from two-copy collective measurements. Observing estimates deviating by less than 1.5% while using only half of the total number of unbiased measurements demonstrates the effectiveness of the ANN-based models.

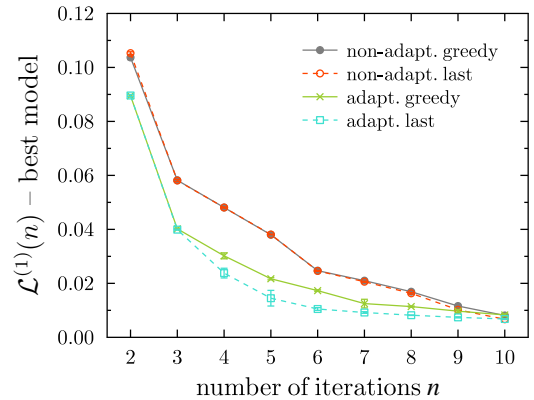


FIG. 3. Comparison of the ANN models for two-qubit systems. Performance in terms of the $\mathcal{L}^{(1)}$ error for all combinations of adaptive/non-adaptive and greedy/last approaches is visualized as a function of the number of n iterations.

Qubit-qutrit states

Similarly to the two-qubit states, we trained and tested models for negativity estimation also on qubit-qutrit systems. In this case, the qubit subsystems of the two copies undergo the non-local $\hat{\Pi}_{\text{Bell}}$ projection and the qutrit subsystems are locally projected. This choice is warranted by the uniqueness of the singlet two-qubit Bell state (the sole anti-symmetric fully entangled state). In this geometry, there are up to 45 unbiased local projections [34]. However, we limit our investigation to $n = 21$ since for a larger number of iterations the training becomes too complex at least given our computation power. One can also argue that there is no point in using two-copy collective measurements if the number of measurements exceeds half of the measurements necessary for standard quantum state tomography. Quantum state tomography of a qubit-qutrit system can be accomplished with 36 measurements.

Using the same two quantifiers $\mathcal{L}^{(1)}$ and R^2 , we assess the performance of the models on the qubit-qutrit states. Numerical values are presented in Tables V and VI for the *greedy* and *last* approaches respectively. Tables VII and VIII provide performances of their non-adaptive counterparts. The resulting trend in terms of the $\mathcal{L}^{(1)}(n)$ measure as a function of the number of iterations n is depicted in Fig. 5. Two-dimensional histograms for a selection of parameters are shown in Fig. 6. Histograms were generated using the same procedure as described in the preceding subsection dedicated to the two-qubit states.

The observations on qubit-qutrit systems are very similar to those of two-qubit systems. The adaptive strategies clearly outperform the non-adaptive approaches. This can be numerically documented, for instance, by considering the best-performing adaptive model for $n = 12$ iterations, which makes estimates that on average deviate

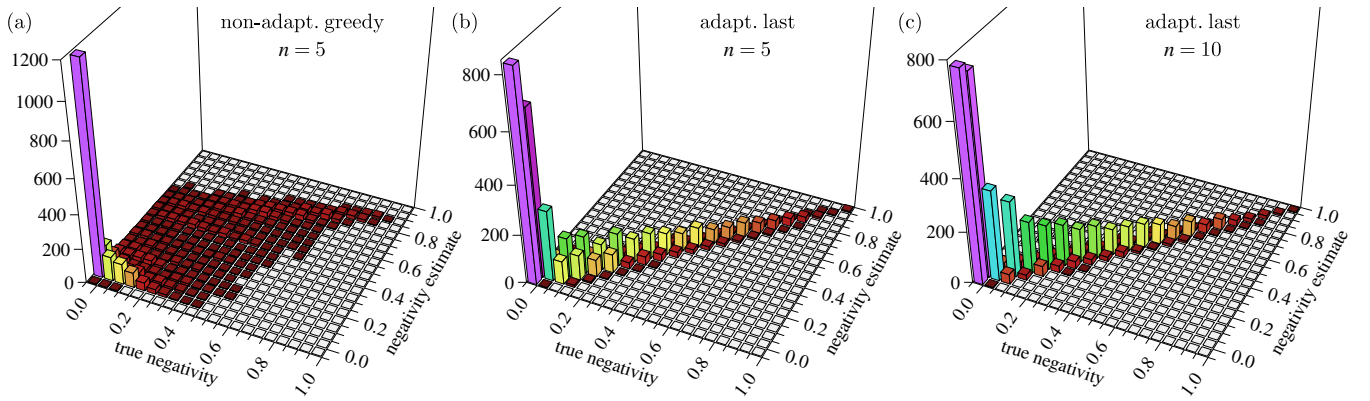


FIG. 4. Histograms showing the distribution of paired values of the true negativity \mathcal{N} and its estimate by the models $\hat{\mathcal{N}}$ in two-qubit systems: (a) the non-adaptive strategy with $n = 5$ iterations, (b) the adaptive *last* approach with $n = 5$ iterations and (c) the adaptive *last* approach with $n = 10$ iterations. Note that ideally only diagonal elements, where $\mathcal{N} = \hat{\mathcal{N}}$, should have non-zero values.

from true negativity values by 0.0184. The non-adaptive model makes errors almost three times bigger (0.0528). Adaptive models trained using the *last* approach again outperform the *greedy* models. No significant difference exists among their non-adaptive equivalents.

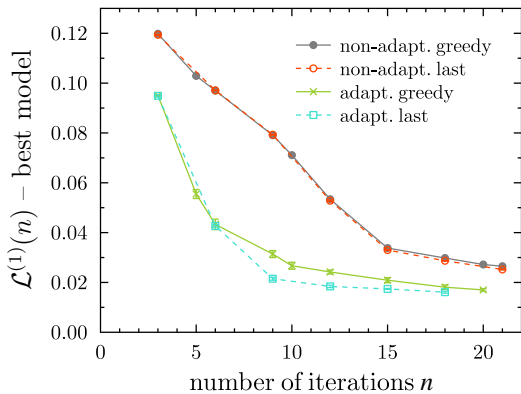


FIG. 5. Comparison of the ANN models for qubit-qutrit systems. Performance in terms of the $\mathcal{L}^{(1)}$ error for all combinations of adaptive/non-adaptive and greedy/last approaches is visualized as a function of the number of n iterations.

CONCLUSIONS

In this study, we investigated the performance of adaptive collective measurement approach to entanglement quantification in two different quantum systems: two-qubit and qubit-qutrit states. We showed that both the *greedy* and *last* adaptive strategies outperformed their non-adaptive counterparts, as expressed in terms of $\mathcal{L}^{(1)}$ errors and the coefficients of determination R^2 . The superiority of adaptive methods is especially pronounced when dealing with a limited number of measurements

TABLE V. Numerical results for qubit-qutrit systems using an adaptive *greedy* measurement strategy as a function of the number of n iterations. The figures of merit $\mathcal{L}^{(1)}$ and R^2 are defined in the main text.

n	$\mathcal{L}^{(1)}$ mean	$\mathcal{L}^{(1)}$ best	R^2 mean	R^2 best
3	0.0953(02)	0.0951	0.7059(33)	0.7084
5	0.0581(18)	0.0555	0.8835(49)	0.8907
6	0.0451(21)	0.0433	0.9269(63)	0.9323
9	0.0329(14)	0.0314	0.9603(34)	0.9641
10	0.0284(14)	0.0267	0.9702(31)	0.9732
12	0.0251(08)	0.0242	0.9767(12)	0.9780
15	0.0218(10)	0.0209	0.9819(16)	0.9836
18	0.0194(09)	0.0181	0.9857(12)	0.9876
20	0.0178(05)	0.0170	0.9878(06)	0.9888

TABLE VI. Numerical results for qubit-qutrit systems using an adaptive *last* measurement strategy as a function of the number of n iterations. The figures of merit $\mathcal{L}^{(1)}$ and R^2 are defined in the main text.

n	$\mathcal{L}^{(1)}$ mean	$\mathcal{L}^{(1)}$ best	R^2 mean	R^2 best
3	0.0954(05)	0.0949	0.7054(16)	0.7039
6	0.0435(05)	0.0427	0.9311(22)	0.9354
9	0.0220(06)	0.0215	0.9812(11)	0.9820
12	0.0192(05)	0.0184	0.9856(07)	0.9870
15	0.0176(02)	0.0174	0.9878(03)	0.9878
18	0.0168(04)	0.0161	0.9890(05)	0.9895

(typically 5 and 12 for the two-qubit and qubit-qutrit systems, respectively). These results suggest that adaptive collective measurements constitute a viable and practical method for entanglement quantification in future quantum communication networks, where resource consumption in terms of measurement configurations is a concern. Note that the two-copy collective measurements discussed in this paper are experimentally quite feasible in communication devices based on entanglement swap-

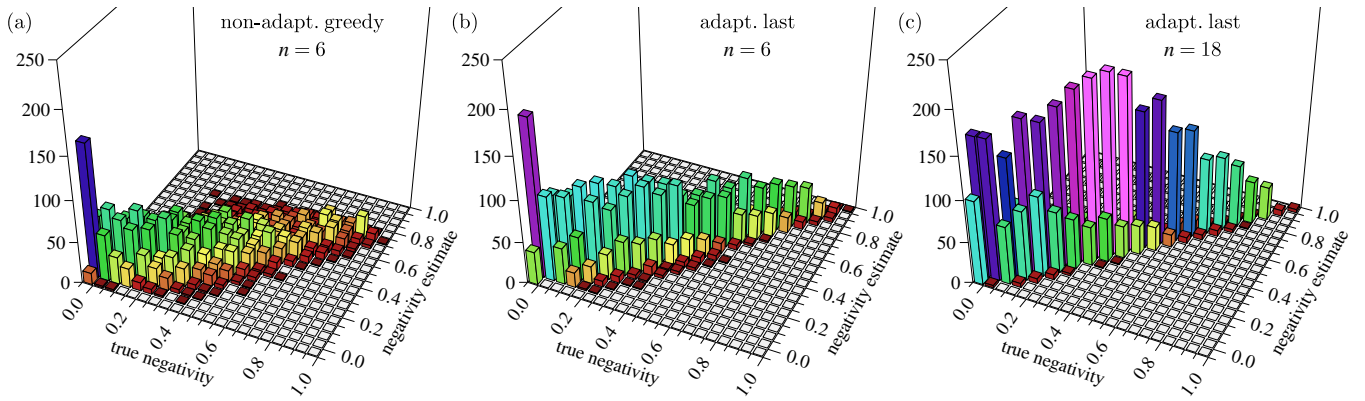


FIG. 6. Histograms showing the distribution of paired values of the true negativity \mathcal{N} and its estimate by the models $\hat{\mathcal{N}}$ in qubit-qutrit systems: (a) the non-adaptive strategy with $n = 6$ iterations, (b) the adaptive *last* approach with $n = 6$ iterations and (c) the adaptive *last* approach with $n = 18$ iterations. Note that ideally only diagonal elements, where $\mathcal{N} = \hat{\mathcal{N}}$, should have non-zero values.

TABLE VII. Numerical results for qubit-qutrit systems using a non-adaptive optimal basis set and the *greedy* estimation approach. Here, n denotes the number of iterations. The figures of merit $\mathcal{L}^{(1)}$ and R^2 are defined in the main text.

n	$\mathcal{L}^{(1)}$ mean	$\mathcal{L}^{(1)}$ best	R^2 mean	R^2 best
3	0.1200(02)	0.1198	0.5665(25)	0.5698
5	0.1034(03)	0.1029	0.6660(15)	0.6678
6	0.0973(02)	0.0970	0.6993(14)	0.7002
9	0.0796(03)	0.0791	0.7798(15)	0.7809
10	0.0712(02)	0.0711	0.8246(10)	0.8247
12	0.0537(02)	0.0534	0.9011(04)	0.9012
15	0.0342(03)	0.0338	0.9580(05)	0.9583
18	0.0300(01)	0.0298	0.9675(05)	0.9679
20	0.0274(02)	0.0272	0.9726(04)	0.9731
21	0.0268(02)	0.0265	0.9737(03)	0.9740

TABLE VIII. Numerical results for qubit-qutrit systems using a non-adaptive optimal basis set and the *last* estimation approach. Here, n denotes the number of iterations. The figures of merit $\mathcal{L}^{(1)}$ and R^2 are defined in the main text.

n	$\mathcal{L}^{(1)}$ mean	$\mathcal{L}^{(1)}$ best	R^2 mean	R^2 best
3	0.1196(02)	0.1194	0.5669(63)	0.5739
6	0.0975(02)	0.0971	0.6984(20)	0.6970
9	0.0795(02)	0.0793	0.7795(17)	0.7798
12	0.0531(03)	0.0528	0.9027(11)	0.9044
15	0.0332(02)	0.0330	0.9598(04)	0.9601
18	0.0288(01)	0.0287	0.9697(03)	0.9700
21	0.0254(02)	0.0252	0.9761(04)	0.9762

ping, such as quantum relays.

As expected, the *last* approach provides somewhat better results, while the *greedy* approach proved easier to train. The best-performing models were able to achieve $\mathcal{L}^{(1)}$ errors below 1.5% with only 5 iterations (measurement configurations) in the case of the two-qubit states and below 2% with 12 iterations in the case of the

qubit-qutrit states. Within the non-adaptive strategies, we did not observe any significant difference between the *greedy* and *last* approaches. In general, the performance obtained meets the requirements for sufficiently small errors, especially considering that other sources of imperfections in typical implementations are on the order of 1 to 2% [57, 58].

In addition to its potential for practical applications, the combination of collective and adaptive measurements also provides opportunities for the future advancement of quantum entanglement quantification. One can, for instance, use this approach to develop practical witnesses for higher-dimensional states or to investigate newly machine-designed entanglement witnesses.

ACKNOWLEDGMENTS

The authors thank CESNET for data management services and J. Cimrman for inspiration. The authors M.Z., J.S. and K.L. acknowledge support by the project of the Czech Science Foundation No. 25-17253S; A.C. and V.T. acknowledge support from the Ministry of Education of the Czech Republic within the OP-JAK project SENDISO no. CZ.02.01.01/00/22_008/0004596.

* martin.zeman01@upol.cz

† travnicekv@fzu.cz

‡ acernoch@fzu.cz

§ jan.soubusta@upol.cz

¶ k.lemr@upol.cz

- [1] A. Einstein, B. Podolsky, and N. Rosen, *Physical Review* **47**, 777 (1935).
- [2] D. Bouwmeester, J.-W. Pan, K. Mattle, M. Eibl, H. Weinfurter, and A. Zeilinger, *Nature* **390**, 575–579 (1997).
- [3] J.-W. Pan, D. Bouwmeester, H. Weinfurter, and

- A. Zeilinger, Phys. Rev. Lett. **80**, 3891 (1998), URL <https://link.aps.org/doi/10.1103/PhysRevLett.80.3891>.
- [4] A. K. Ekert, Phys. Rev. Lett. **67**, 661–663 (1991).
- [5] B. C. Hiesmayr, Scientific Reports **11**, 19739 (2021), URL <https://doi.org/10.1038/s41598-021-98523-6>.
- [6] S. Gharibian, Quantum Information & Computation **10**, 343–360 (2010).
- [7] G. Vidal and R. F. Werner, Physical Review A **65**, 032314 (2002), ISSN 1094-1622, URL <http://dx.doi.org/10.1103/PhysRevA.65.032314>.
- [8] A. Peres, Physics Letters A **128**, 19 (1988), ISSN 0375-9601, URL <https://www.sciencedirect.com/science/article/pii/0375960188910341>.
- [9] A. Peres, Phys. Rev. Lett. **77**, 1413 (1996), URL <https://link.aps.org/doi/10.1103/PhysRevLett.77.1413>.
- [10] G. Jaeger, *Quantum information: an overview* (Springer, 2010).
- [11] R. Horodecki, P. Horodecki, M. Horodecki, and K. Horodecki, Rev. Mod. Phys. **81**, 865 (2009), URL <https://link.aps.org/doi/10.1103/RevModPhys.81.865>.
- [12] M. Ježek, J. Fiurášek, and Z. Hradil, Phys. Rev. A **68**, 012305 (2003), URL <https://link.aps.org/doi/10.1103/PhysRevA.68.012305>.
- [13] A. Miranowicz, K. Bartkiewicz, J. Peřina, M. Koashi, N. Imoto, and F. Nori, Phys. Rev. A **90**, 062123 (2014), URL <https://link.aps.org/doi/10.1103/PhysRevA.90.062123>.
- [14] A. Acín, R. Tarrach, and G. Vidal, Phys. Rev. A **61**, 062307 (2000), URL <https://link.aps.org/doi/10.1103/PhysRevA.61.062307>.
- [15] F. A. Bovino, G. Castagnoli, A. Ekert, P. Horodecki, C. M. Alves, and A. V. Sergienko, Phys. Rev. Lett. **95**, 240407 (2005), URL <https://link.aps.org/doi/10.1103/PhysRevLett.95.240407>.
- [16] S. Walborn, P. Souto Ribeiro, L. Davidovich, F. Mintert, and A. Buchleitner, Nature **440**, 1022 (2006).
- [17] L. Rudnicki, P. Horodecki, and K. Życzkowski, Phys. Rev. Lett. **107**, 150502 (2011), URL <https://link.aps.org/doi/10.1103/PhysRevLett.107.150502>.
- [18] L. Rudnicki, Z. Puchała, P. Horodecki, and K. Życzkowski, Phys. Rev. A **86**, 062329 (2012), URL <https://link.aps.org/doi/10.1103/PhysRevA.86.062329>.
- [19] K. Lemr, K. Bartkiewicz, and A. Černocho, Phys. Rev. A **94**, 052334 (2016), URL <https://link.aps.org/doi/10.1103/PhysRevA.94.052334>.
- [20] P. Horodecki and A. Ekert, Phys. Rev. Lett. **89**, 127902 (2002), URL <https://link.aps.org/doi/10.1103/PhysRevLett.89.127902>.
- [21] R. Filip, Phys. Rev. A **65**, 062320 (2002), URL <https://link.aps.org/doi/10.1103/PhysRevA.65.062320>.
- [22] J. Fiurášek, Phys. Rev. A **66**, 052315 (2002), URL <https://link.aps.org/doi/10.1103/PhysRevA.66.052315>.
- [23] K. Bartkiewicz, G. Chimczak, and K. Lemr, Phys. Rev. A **95**, 022331 (2017), URL <https://link.aps.org/doi/10.1103/PhysRevA.95.022331>.
- [24] J. Roik, K. Bartkiewicz, A. Černocho, and K. Lemr, Phys. Rev. Appl. **15**, 054006 (2021), URL <https://link.aps.org/doi/10.1103/PhysRevApplied.15.054006>.
- [25] J. Roik, K. Bartkiewicz, A. Černocho, and K. Lemr, Physics Letters A **446**, 128270 (2022), ISSN 0375-9601, URL <https://www.sciencedirect.com/science/article/pii/S0375960122003528>.
- [26] K. Hornik, M. Stinchcombe, and H. White, Neural Networks **2**, 359 (1989), ISSN 0893-6080, URL <https://www.sciencedirect.com/science/article/pii/0893608089900208>.
- [27] J.-W. Pan, D. Bouwmeester, H. Weinfurter, and A. Zeilinger, Phys. Rev. Lett. **80**, 3891 (1998), URL <https://link.aps.org/doi/10.1103/PhysRevLett.80.3891>.
- [28] H.-J. Briegel, W. Dür, J. I. Cirac, and P. Zoller, Phys. Rev. Lett. **81**, 5932 (1998), URL <https://link.aps.org/doi/10.1103/PhysRevLett.81.5932>.
- [29] B. C. Jacobs, T. B. Pittman, and J. D. Franson, Phys. Rev. A **66**, 052307 (2002), URL <https://link.aps.org/doi/10.1103/PhysRevA.66.052307>.
- [30] R. Bassoli, H. Boche, C. Deppe, R. Ferrara, F. H. P. Fitzek, G. Janssen, and S. Saeeedinaeni, *Quantum Communication Networks* (Springer, 2021).
- [31] V. Trávníček, K. Bartkiewicz, A. Černocho, and K. Lemr, Phys. Rev. Appl. **14**, 064071 (2020), URL <https://link.aps.org/doi/10.1103/PhysRevApplied.14.064071>.
- [32] L. Conlon, T. Vogl, C. Marciniak, I. Pogorelov, S. Yung, F. Eilenberger, D. Berry, F. Santana, R. Blatt, T. Monz, et al., Nature Physics **19**, 1 (2023).
- [33] V. Trávníček, K. Bartkiewicz, A. Černocho, and K. Lemr, Phys. Rev. Lett. **123**, 260501 (2019), URL <https://link.aps.org/doi/10.1103/PhysRevLett.123.260501>.
- [34] V. Trávníček, J. Roik, K. Bartkiewicz, A. Černocho, P. Horodecki, and K. Lemr, Phys. Rev. Res. **6**, 033056 (2024), URL <https://link.aps.org/doi/10.1103/PhysRevResearch.6.033056>.
- [35] S. Abo, J. Soubusta, K. Jiráková, K. Bartkiewicz, A. Černocho, K. Lemr, and A. Miranowicz, Scientific Reports **13**, 8564 (2023), URL <https://doi.org/10.1038/s41598-023-35015-9>.
- [36] J. Soubusta, A. Černocho, and K. Lemr, Physics Letters A **559**, 130911 (2025), ISSN 0375-9601, URL <https://www.sciencedirect.com/science/article/pii/S0375960125006917>.
- [37] A. Hentschel and B. C. Sanders, in *2010 Seventh International Conference on Information Technology: New Generations* (2010), pp. 506–511.
- [38] D. G. Fischer, S. H. Kienle, and M. Freyberger, Phys. Rev. A **61**, 032306 (2000), URL <https://link.aps.org/doi/10.1103/PhysRevA.61.032306>.
- [39] T. Hannemann, D. Reiss, C. Balzer, W. Neuhauser, P. E. Toschek, and C. Wunderlich, Phys. Rev. A **65**, 050303 (2002), URL <https://link.aps.org/doi/10.1103/PhysRevA.65.050303>.
- [40] C. J. Happ and M. Freyberger, Phys. Rev. A **78**, 064303 (2008), URL <https://link.aps.org/doi/10.1103/PhysRevA.78.064303>.
- [41] F. Huszár and N. M. T. Houlby, Phys. Rev. A **85**, 052120 (2012), URL <https://link.aps.org/doi/10.1103/PhysRevA.85.052120>.
- [42] G. I. Struchalin, I. A. Pogorelov, S. S. Straupe, K. S. Kravtsov, I. V. Radchenko, and S. P. Kulik, Phys. Rev. A **93**, 012103 (2016), URL <https://link.aps.org/doi/10.1103/PhysRevA.93.012103>.
- [43] Y. Quek, S. Fort, and H. K. Ng, npj Quantum Information **7**, 105 (2021).
- [44] A. Gaikwad, O. Bihani, Arvind, and K. Dorai, Phys. Rev. A **109**, 012402 (2024), URL <https://link.aps.org/doi/10.1103/PhysRevA.109.012402>.

- org/doi/10.1103/PhysRevA.109.012402.
- [45] D. T. Pope, H. M. Wiseman, and N. K. Langford, Phys. Rev. A **70**, 043812 (2004), URL <https://link.aps.org/doi/10.1103/PhysRevA.70.043812>.
- [46] N. Linden and R. de Wolf, *Adaptive quantum phase estimation can be better than non-adaptive* (2025), 2511.05372, URL <https://arxiv.org/abs/2511.05372>.
- [47] J. G. Smith, C. H. W. Barnes, and D. R. M. Arvidsson-Shukur, Phys. Rev. A **109**, 042412 (2024), URL <https://link.aps.org/doi/10.1103/PhysRevA.109.042412>.
- [48] S. Lerch and A. Stefanov, Opt. Lett. **39**, 5399 (2014), URL <https://opg.optica.org/ol/abstract.cfm?URI=ol-39-18-5399>.
- [49] M. Weilenmann, E. Aguilar, and M. Navascues, Nature Communications **12**, 4553 (2021).
- [50] J. Pauwels, S. Pironio, E. Z. Cruzeiro, and A. Tavakoli, Phys. Rev. Lett. **129**, 120504 (2022), URL <https://link.aps.org/doi/10.1103/PhysRevLett.129.120504>.
- [51] S. Hochreiter and J. Schmidhuber, Neural Computation **9**, 1735 (1997).
- [52] R. Pascanu, Y. Yere, T. Mikolov, and Y. Rachmad, 30th International Conference on Machine Learning, ICML 2013, cycle 3 pp. 1310–1318 (2012).
- [53] J. Maziero, Brazilian Journal of Physics **45**, 575–583 (2015), ISSN 1678-4448, URL <http://dx.doi.org/10.1007/s13538-015-0367-2>.
- [54] S. L. Smith, P.-J. Kindermans, C. Ying, and Q. V. Le, *Don't decay the learning rate, increase the batch size* (2018), 1711.00489, URL <https://arxiv.org/abs/1711.00489>.
- [55] A. Paszke, S. Gross, F. Massa, A. Lerer, J. Bradbury, G. Chanan, T. Killeen, Z. Lin, N. Gimelshein, L. Antiga, et al., *Pytorch: An imperative style, high-performance deep learning library* (2019), 1912.01703, URL <https://arxiv.org/abs/1912.01703>.
- [56] M. Zeman, V. Trávníček, A. Černoch, J. Soubusta, and K. Lemr, Figshare repository (2026), URL <https://doi.org/10.6084/m9.figshare.31861405>.
- [57] A. Černoch, K. Bartkiewicz, K. Lemr, and J. Soubusta, Phys. Rev. A **97**, 042305 (2018), URL <https://link.aps.org/doi/10.1103/PhysRevA.97.042305>.
- [58] K. Jiráková, A. Barasiński, A. Černoch, K. Lemr, and J. Soubusta, Phys. Rev. Applied **16**, 054042 (2021), URL <https://link.aps.org/doi/10.1103/PhysRevApplied.16.054042>.